*Chinese Journal of*
**POLYMER SCIENCE**

RESEARCH ARTICLE

https://doi.org/10.1007/s10118-026-3722-6
*Chinese J. Polym. Sci.*

# Three-in-One Coupled Shape Memory, Self-healing, and Photochromic System in Dynamic Covalent Polyurethane Network for Sequential 4D Encryption

Yi-Xin Ji[a], Ahmed Olalekan Omoniyi[a,b], Yang Zhou[c*], Ying-Chao Zhang[d*], and Jian-Fu Zhang[a*]

[a] *Jilin Provincial Science and Technology Innovation Centre of Optical Materials and Chemistry, School of Chemistry and Environmental Engineering, Changchun University of Science and Technology, Changchun 130022, China*
[b] *Zhongshan Institute of Changchun University of Science and Technology, Zhongshan 528437, China*
[c] *School of Opto-electronic Engineering, Changchun University of Science and Technology, Changchun 130022, China*
[d] *Shandong Province Engineering Research Center for Future Industries of Key Materials in Optoelectronics, Weifang University of Science and Technology, Shouguang 262700, China*

Electronic Supplementary Information

**Abstract** Information leakage and forgery continue to threaten the security of the information storage and transmission. However, most existing physical encryption materials rely on single and predictable stimulus-response mechanisms, resulting in limited security, programmability, and service life. Herein, a high-security sequential 4D encryption system is developed based on a dynamic covalent polyurethane network that integrates shape memory, self-healing, and photochromism in one system. Arylboronic acid was incorporated into the polyurethane framework to form a dynamic boron carbamate network. The resulting boroxine crosslinks act as reversible junctions, enabling thermally triggered shape memory behavior, while simultaneously providing efficient self-healing through reversible hydrolysis and reformation. The optimized polyurethane exhibited a tensile strength of about 35 MPa, a shape-fixity ratio of >99%, and a shape-recovery ratio of up to 83% while achieving a self-healing efficiency of about 81% after thermal treatment. In parallel, the incorporation of a photochromic dye enables precise time-dependent color evolution under ultraviolet irradiation. The synergistic coupling of thermal and photonic responses allows sequential and time-gated information decoding, significantly increasing the encryption complexity and resistance to unauthorized access. The resulting films function as dynamic 4D encryption carriers from which correct information can be retrieved only through a predefined sequence of shape recovery and color transformation. This study provides a versatile strategy for next-generation physical encryption materials with intrinsic damage tolerance, long-term reliability, and storage potential in optical data storage and advanced anti-counterfeiting applications.

**Keywords** Information encryption; Multistimuli response; Dynamic bond; Polyurethane

**Citation:** Ji, Y. X.; Omoniyi, A. O.; Zhou, Y.; Zhang, Y. C.; Zhang, J. F. Three-in-one coupled shape memory, self-healing, and photochromic system in dynamic covalent polyurethane network for sequential 4D encryption. *Chinese J. Polym. Sci.* https://doi.org/10.1007/s10118-026-3722-6

## INTRODUCTION

With the rapid development of the digital era and big data technologies, secure information storage, transmission, and authentication have become indispensable in modern society, spanning economic activities, scientific research, and public safety systems.[1–3] However, the continuous evolution of counterfeiting, duplication, and simulation technologies has significantly increased the risk of information leakage and forgery, leading to substantial economic losses and security vulnerabilities.[4–6] These challenges highlight the urgent need for advanced physical encryption materials that are capable of providing higher security levels than conventional digital encryption strategies. Most existing physical encryption systems rely on single stimulus-response mechanisms such as color changes triggered by light,[7–12] heat,[13–16] humidity,[17–19] and pressure.[20–23] Although effective for hiding basic information, these two-dimensional (2D) encryption modes suffer from inherent security limitations, as encrypted information can often be decoded by direct exposure to a single external stimulus.[24,25] To improve encryption complexity, three-dimensional (3D) encryption strategies that combine surface patterns with macroscopic shape transformations have been proposed.[26,27] However, static 3D structures remain vulnerable to reverse engineering-, replication-, and simulation-based attacks. Even advanced physically unclonable functions (PUFs), while theoretically secure, may face modeling or machine-learning-assisted simulation threats.[28–30]

* Corresponding authors, E-mail: zhouyang@cust.edu.cn (Y.Z.)
E-mail: zhangyingchao@wfust.edu.cn (Y.C.Z.)
E-mail: zhangjianfu@cust.edu.cn (J.F.Z.)
Received February 13, 2026; Accepted April 20, 2026; Published online July 20, 2026

To address these limitations, four-dimensional (4D) encryption has emerged as an advanced strategy that introduces time as an additional encryption dimension, enabling information to evolve dynamically under controlled stimulus sequences.[31–33] Unlike static encryption systems, 4D encryption significantly enhances the information complexity, unpredictability, and resistance to brute-force or simulation attacks.[34–38] Nevertheless, realizing practical 4D encryption materials remains challenging, as it requires precise coordination between reversible shape programmability, time-dependent information evolution, and long-term material reliability within a single-material platform. From a material perspective, two key requirements must be satisfied to achieve an effective 4D encryption. First, the material must possess a reversibly programmable shape transformation that allows encrypted information to remain concealed until the correct stimulus sequence is applied. Shape memory polymers (SMPs) fulfill this requirement by enabling programmable temporary shapes to recover to a permanent shape under external stimuli such as light, heat, and electricity.[39–44] Typical SMPs rely on a dual-phase architecture consisting of a stable cross-linking point that stores the permanent shape and reversible switching segments that enable temporary shape fixation and recovery. This reversible deformation mechanism offers a powerful means of protecting information during storage and transmission. Second, 4D encryption requires a dynamic, time-dependent information output, in which multiple layers of information are revealed sequentially rather than simultaneously. Materials exhibiting a serialized response, such as a shape change followed by color evolution, can encode multidimensional information within a single object. Such dynamic information cannot be fully captured by one-time characterization methods (*e.g.*, optical microscopy or spectroscopy), which provide intrinsic resistance to physical replication and reverse engineering.[45–47] However, integrating these two requirements into a single-material system without mutual interference between response mechanisms remains a significant challenge.

Polyurethane (PU) has emerged as a highly attractive matrix for SMP-based encryption systems due to its versatile molecular design, tunable mechanical properties, and excellent processability.[48–51] In particular, waterborne polyurethane (WPU) offers additional advantages, including environmental friendliness and scalable fabrication. Nevertheless, conventional PU-based SMPs suffer from an inherent limitation: repeated deformation cycles and unavoidable external damage often induce microcracks or macroscopic fractures, leading to irreversible mechanical degradation and loss of shape memory functionality.[52] Self-healing materials have been developed to overcome this bottleneck by enabling damage repair through reversible interactions.[53,54] Existing self-healing strategies primarily rely on dynamic covalent bonds (such as disulfide bonds,[55–57] borate ester bonds,[58–60] *etc.*) or non-covalent bonds (such as hydrogen bonds, metal coordination, host-guest interactions, *etc.*).[61–63] Among these, dynamic covalent networks are particularly attractive because of the balance between mechanical robustness and reversibility. Consequently, integrating self-healing capability into SMPs to form self-healing shape memory polymers has become an important research direction, aiming to extend the service life while maintaining functional reliability.[64–66] Despite recent progress, reports combining self-healing, shape memory, and time-dependent optical encryption within a single polymer network remain limited.

Herein, we report a dynamic covalent polyurethane network that integrates shape memory, self-healing, and photochromism to construct a high-security sequential 4D encryption system. WPU was synthesized using 3-aminophenylboronic acid (APBA) as a functional end-capping agent to introduce dynamic boron carbamate units. Upon dehydration, the boronic acid moieties reversibly form tripodal boroxines, which serve as stable yet dynamic junctions acting simultaneously as permanent shape memory netpoints and self-healing sites through reversible hydrolysis–reformation processes (Schemes 1a and 1b). The semicrystalline polycaprolactone (PCL) segments function as reversible switching domains, enabling thermally triggered shape programming and recovery. Furthermore, the incorporation of a photochromic dye, 2,2'-dinaphthylamine (CDP), endows the system with time-dependent color evolution under ultraviolet irradiation. By coupling thermally induced shape recovery with light-triggered color changes, a time-gated 4D encryption platform was achieved, enabling controlled information writing, sequential decoding, and irreversible information erasure (Scheme 1c). This study demonstrates a synergistic material design strategy that integrates multimodal encryption, intrinsic damage tolerance, and long-term reliability, offering a promising route toward next-generation physical encryption, optical data storage, and advanced anti-counterfeiting technologies.

## EXPERIMENTAL

### Materials

Isophorone diisocyanate (IPDI, 99%), dibutyltin dilaurate (95%), 2,2-bis(hydroxymethyl)propionic acid (DMPA, 98%), 3-aminobenzeneboronic acid (APBA, 99.5%), dodecyl sodium sulfonate, and 2,2-dinaphthylamine (CDP) were purchased from Rhawn (Shanghai, China). Poly(ε-caprolactone) (PCL 2105, $M_w$=1000 Da) was purchased from Hunan Juren Chemical Nova Technology Co., (Hunan, China). The PCL and DMPA were dried under vacuum at 80 °C for 24 h before use. All the other materials were used as supplied. Laboratory-made deionized water was used as the continuous phase during emulsification.

### Preparation of Aminophenylboronic Acid Functionalized Waterborne Polyurethane (WPU-APBA) Emulsion

The WPU was synthesized using 2-butanone to adjust the viscosity of the reaction system. IPDI, PCL, and DMPA were added to a 1000 mL three-neck flask and stirred at 300 r/min. Dibutyltin dilaurate was heated to 80 °C for 3 h. Subsequently, APBA was added and the reaction mixture was stirred for 2 h to facilitate end-capping. The reaction mixture was then cooled to 55 °C, neutralized with triethylamine, and stirred at 700 r/min for 0.5 h. To enhance emulsification, dodecyl sodium sulfonate was added, and the mixture was stirred at 1200 r/min for 0.5 h, cooled to 50 °C, supplemented with deionized water, and fully emulsified at 1400 r/min for 1 h. Finally, 2-butanone was re-

https://doi.org/10.1007/s10118-026-3722-6

moved by rotary evaporation at 55 °C to obtain a WPU-APBA emulsion with a solid content of about 35%. The optimum emulsion was determined by adjusting the soft segment and APBA contents to create different emulsion systems of WPU-APBA-0.3, WPU-APBA-0.5, WPU-APBA-1, WPU-APBA-3 and WPU-APBA-5, as listed in Table S1 (in the electronic supplementary information, ESI).

## Preparation of Photochromic Polyurethane Emulsions

To prepare the photochromic polyurethane emulsion, CDP was added to the WPU-APBA-0.5 emulsion. The mixture was stirred at 300 r/min for 24 h at room temperature to obtain a mixed APBA-CDP emulsion.

## Preparation of Polyurethane Films

Polyurethane films were prepared by casting a measured amount of the emulsion into a polytetrafluoroethylene (PTFE) mold (1 cm radius). The cast emulsion was allowed to dry naturally at room temperature, yielding uniform films that were suitable for subsequent characterization and functional testing.

## Characterization

$^1$H-NMR spectra were recorded at 25 °C using a 500 MHz spectrometer (Bruker DRX AVANCE III, Bruker, Switzerland). Fourier transform infrared (FTIR) spectra were recorded using an FTIR-8400S instrument (Shimadzu, Japan), with air as the background reference. The film crystallinity was probed using X-ray diffraction (XRD; Panaco Cangtian) with a scan range of 5°–60°. The weight-average molecular weight ($M_w$), number-average molecular weight ($M_n$), and polydispersity index (PDI) were determined using gel permeation chromatography (GPC; 515 HPLC Pump Waters Company, USA) with tetrahydrofuran as the solvent. The tensile strength was measured using an electronic universal testing machine (PT14-014, 20 kN, China) at a load change rate of 20 N/s and displacement rate of 40 mm/min. Thermogravimetric analysis (TGA; TGDTA 7300, HITACHI, Japan) was conducted over a temperature range of 20–800 °C under a nitrogen purge rate of 10 mL/min. Dynamic mechanical analysis (DMA; Q800, TA, USA) was performed in three-point bending mode at a ramp rate of 10 °C/min and a frequency of 1 Hz in the temperature range from –80 °C to 100 °C. $T_g$ was defined as the peak of the tan$\delta$ curve. The thermal stabilities of the samples were determined using differential scanning calorimetry (DSC) and a TA DSC-2500 (TA Instruments, USA). The samples were sealed in an aluminum crucible and tested under nitrogen atmosphere at a flow rate of 50 mL/min. To eliminate any prior thermal history, deliberate heating and annealing processes were used. During the heating cycle, the sample was heated at a rate of 10 °C/min in the temperature range from –80 °C to 100 °C and annealed at 100 °C for 10 min to remove the residual effects of the previous heat treatment. During the cooling pro-

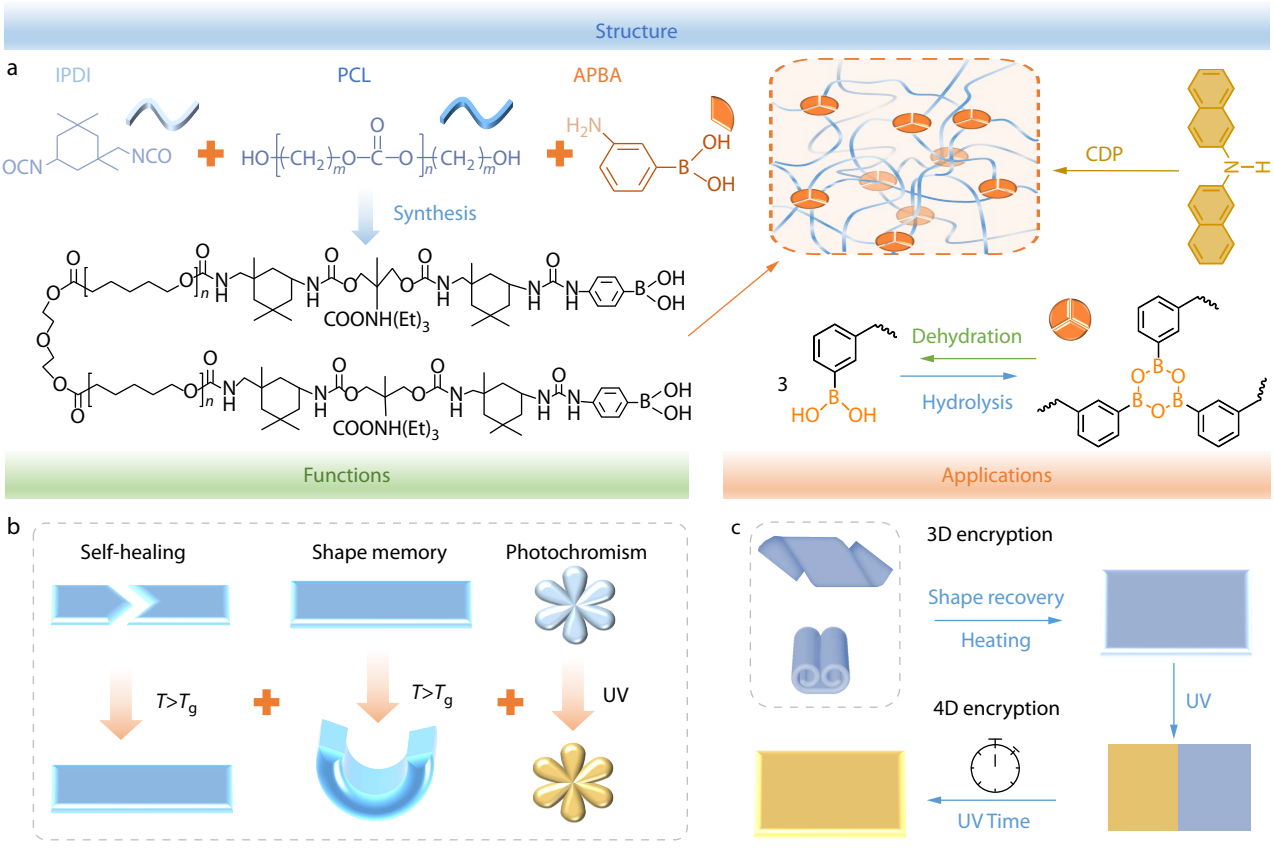


**Scheme 1** Design and application of a dynamic covalent polyurethane-based sequential 4D encryption system. (a) Schematic synthesis of the polyurethane network with reversible transformation of boroxine crosslinks; (b) Structure-function relationship illustrating thermally triggered shape memory, dynamic boroxine-enabled self-healing, and UV-induced photochromism; (c) Illustration of 3D encryption *via* shape recovery and advanced time-gated 4D encryption achieved by sequential shape recovery and UV-controlled color evolution.

https://doi.org/10.1007/s10118-026-3722-6

cess, the sample was cooled to −80 °C, at a scanning rate of 10 °C/min. This controlled cooling process provides insight into the behavior of the material during cooling and the potential phase transition.

The shape memory properties of the composites were quantitatively evaluated by DMA in the tensile mode under controlled stress conditions. samples were heated to 70 °C for 3 min, stretched to 40% strain, and shape-fixed at 0 °C while maintaining constant stress. After the stress release, the samples were reheated to 70 °C and held isothermally for 25–30 min. To test the self-healing ability, the polyurethane sample was cut out with a knife, the cross section was dipped in water, kept in contact with its complementary half, and then heated to 80 °C to repair the damage.

## RESULTS AND DISCUSSION

### Molecular Design and Structural Characterization of Phenylboronic Acid Ester-based Polyurethane

To simultaneously achieve shape memory behavior and self-healing capability within a single polymer network, a segmented polyurethane architecture was rationally designed. IPDI was selected as the hard segment to form a mechanically strong and ordered microdomain, whereas semicrystalline PCL served as the soft segment to realize microphase separation and reversible chain mobility. Thus, APBA was introduced as a functional capping agent, yielding a dynamic covalent polyurethane network with boron carbamate linkages, denoted as WPU-APBA. During film formation from a polyurethane emulsion, the pendant phenylboronic acid groups undergo reversible dehydration and trimerization to form tripodal boroxines.[58,60] Upon damage and subsequent thermal treatment, the residual boronic acid groups at the fractured interfaces recondense to regenerate boroxine crosslinks, while elevated temperatures simultaneously enhance segmental mobility, facilitating interfacial diffusion and bond reformation. As a result, the hard segments composed of IPDI and APBA function as a stationary phase for shape memory and a self-healing bonding point through reversible tripodal boroxine hydrolysis–reformation. Meanwhile, the semi-crystalline PCL domains act as flexible segments, providing the reversible phase required for shape programming and recovery as well as facilitating molecular movement across damaged interfaces. This synergistic dual-dynamic cross-linked network enabled efficient self-healing and stable shape memory performance.

To investigate the influence of APBA content on the network structure and properties, a series of WPU-APBA samples with varying APBA-to-soft-segment ratios (WPU-APBA-*x*, *x*=0.3, 0.5, 1, 3, and 5) were prepared. The specific blending ratios and synthesis routes are presented in Table S1 and Fig. S1 (in ESI), respectively. The successful synthesis of WPU-APBA was confirmed using FTIR and $^1$H-NMR spectroscopy. As shown in Fig. 1(a), the disappearance of the characteristic isocyanate absorption band at 2270 cm$^{-1}$ indicates the complete consumption of the —NCO groups. The presence of a strong carbonyl stretching band at 1735 cm$^{-1}$ is attributed to the stretching vibration of the carbonyl group in carbamate, while the absorption band at 710 cm$^{-1}$ is assigned to the characteristic vibration of $B_3O_3$ tripodal boroxines, indicating the formation of dynamic boron-oxygen crosslinks.[67] These results, together with $^1$H-NMR (Fig. S2 in ESI) and GPC analysis (Table S2 in ESI) to verify the successful incorporation of APBA into the polyurethane backbone.[68] The introduction of APBA influences the intermolecular interactions within the polymer network. The FTIR spectra of the WPU-APBA-*x* samples (Fig. 1b) and deconvolution analysis of the C=O stretching region (1600–1800 cm$^{-1}$) revealed a progressive enhancement of hydrogen bonding with increasing APBA content (Fig. 1c and Figs. S3–S6 in ESI). The carbonyl bands were deconvoluted into free, disordered, and ordered hydrogen-bonded C=O components using a Gaussian function, with the quantitative fitting parameters summarized in Table S3 (in ESI).[69–71] The proportion of hydrogen-bonded C=O groups increased from 49.93% to 64.71% as APBA content increased, thereby strengthening microphase separation and network cohesion.

Mechanical integrity is a prerequisite for reliable stimulus-responsive behavior, particularly for repeated programming and recovery. Tensile testing of the WPU-APBA films (Fig. 1d) reveals that the mechanical performance initially improved with increasing APBA content due to enhanced crosslinking density and intermolecular interactions. However, excessive APBA loading (>1 wt%) led to a decline in the tensile strength and elongation at break. This reduction is attributed to the increased rigidity and restricted segmental mobility imposed by excessive boroxine crosslinks, which compromise the network toughness of WPU-APBA. Among all compositions, WPU-APBA-1 exhibited optimal mechanical performance, with a tensile strength of 35.23 MPa and an elongation at break of 855%, demonstrating a balanced combination of strength and flexibility suitable for reversible deformation processes. Thermal stability is critical for materials subjected to repeated thermal activation during shape memory and self-healing cycles. Thermogravimetric analysis (TGA in Fig. 1e) shows that all WPU-APBA samples exhibit high thermal stability, with initial decomposition occurring at 250 °C and main degradation occurring between 300 and 500 °C, corresponding to urethane bond cleavage and backbone depolymerization. The elevated decomposition temperatures indicated that strong boric-containing interactions contributed to the stabilization of the polymer network under thermal stress. The fluidity of the molecular chain significantly influences the mobility of the polyurethane chain during the shape memory process. To better understand the fluidity and viscoelastic behavior of the molecular chain, the dynamic mechanical properties of different polyurethane samples were evaluated using DMA, as shown in Fig. 1(f). At low temperatures, the high storage modulus ($E'$) reflects a rigid glassy state with frozen chain segments. As the temperature increased, a sharp decline in $E'$ corresponded to the glass transition of the material, indicating the activation of segmental mobility. Above the glass transition temperature ($T_g$), a rubbery plateau emerged, reflecting the stable network elasticity governed by boroxine crosslinks. This temperature-dependent modulus evolution confirms that the synthesized WPU-APBA networks possess the necessary thermal and mechanical characteristics to support a reliable shape memory behavior.

### Shape-programmable Self-healing Polyurethane Film

According to the DMA results (Fig. 1f and Fig. S7 in ESI), the $T_g$ of the WPU-APBA samples varied with the APBA content, ranging

https://doi.org/10.1007/s10118-026-3722-6

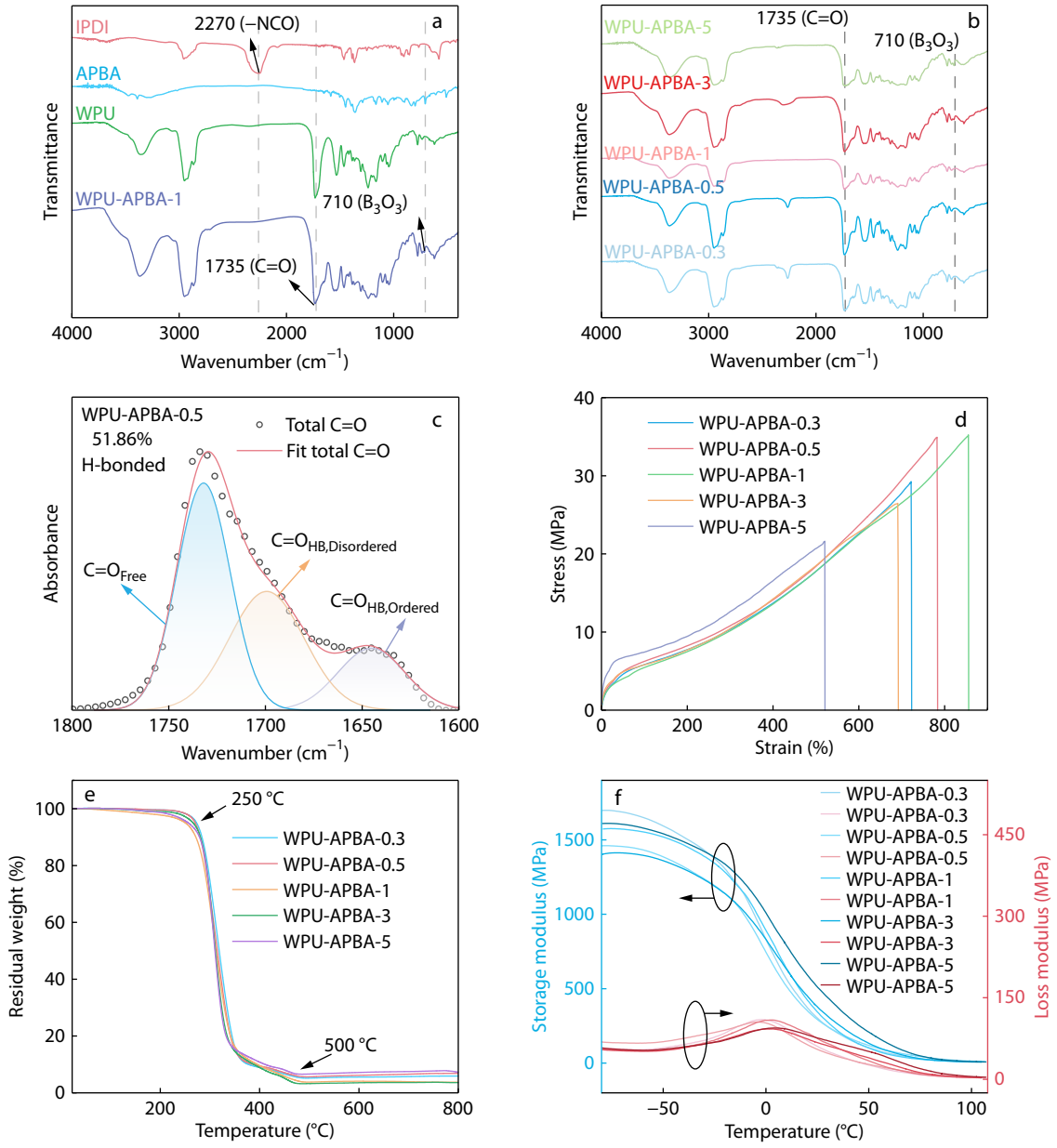


**Fig. 1** Structural, mechanical, and thermal characterization of WPU-APBA. (a) Fourier transform infrared (FTIR) spectra confirming urethane formation and boroxine crosslinking; (b) FTIR spectra of WPU-APBA-*x*; (c) Deconvoluted carbonyl stretching region of WPU-APBA-0.5; (d) Tensile stress-strain curves of WPU-APBA-*x* films; (e) TGA thermograms and (f) storage and loss moduli of WPU-APBA-*x* films.

from 57 °C to 94 °C. Studies on boron-oxygen heterocyclic dynamic polymers have shown that effective bond exchange typically requires temperatures of 70–80 °C.[72,73] Therefore, 80 °C was selected as the self-healing temperature to ensure a sufficient chain mobility for interfacial diffusion and entanglement. The self-healing tests of WPU-APBA-*x* at 60 °C for 1h (Fig. S8 and Table S4 in ESI) further confirmed that lower temperatures are not suitable for effective healing. To evaluate the healing performance, the WPU-APBA-*x* films were cut into two pieces, lightly wetted at the fractured interface to activate boroxine hydrolysis, recontacted, and heated at 80 °C for 1 h to promote recrosslinking. As shown in Fig. 2(a), the scratch gradually disappeared with healing time, indicating progressive interfacial reconnection. The incorporation of APBA introduces dynamic boronic acid moieties that undergo reversible dehydration to form boroxine ($B_3O_3$) crosslinks during the film formation. Boroxine is a trimeric boron–oxygen ring structure that can reversibly hydrolyze in the presence of water and reform upon drying or heating (Fig. 2b). This dynamic covalent equilibrium enables bond exchange across damaged interfaces, thereby imparting an intrinsic self-healing capability to the polyurethane network. A quantitative assessment was performed by comparing the tensile strength before and after healing (Fig. 2c). The healing efficiency increased with APBA content with WPU-APBA-3 reaching a maximum of 80.66%, and then decreased at 5 wt% loading (69.42%). This trend reflects the balance between dynamic bond density and network rigidity; moderate APBA enhances interfacial bond exchange, whereas excessive

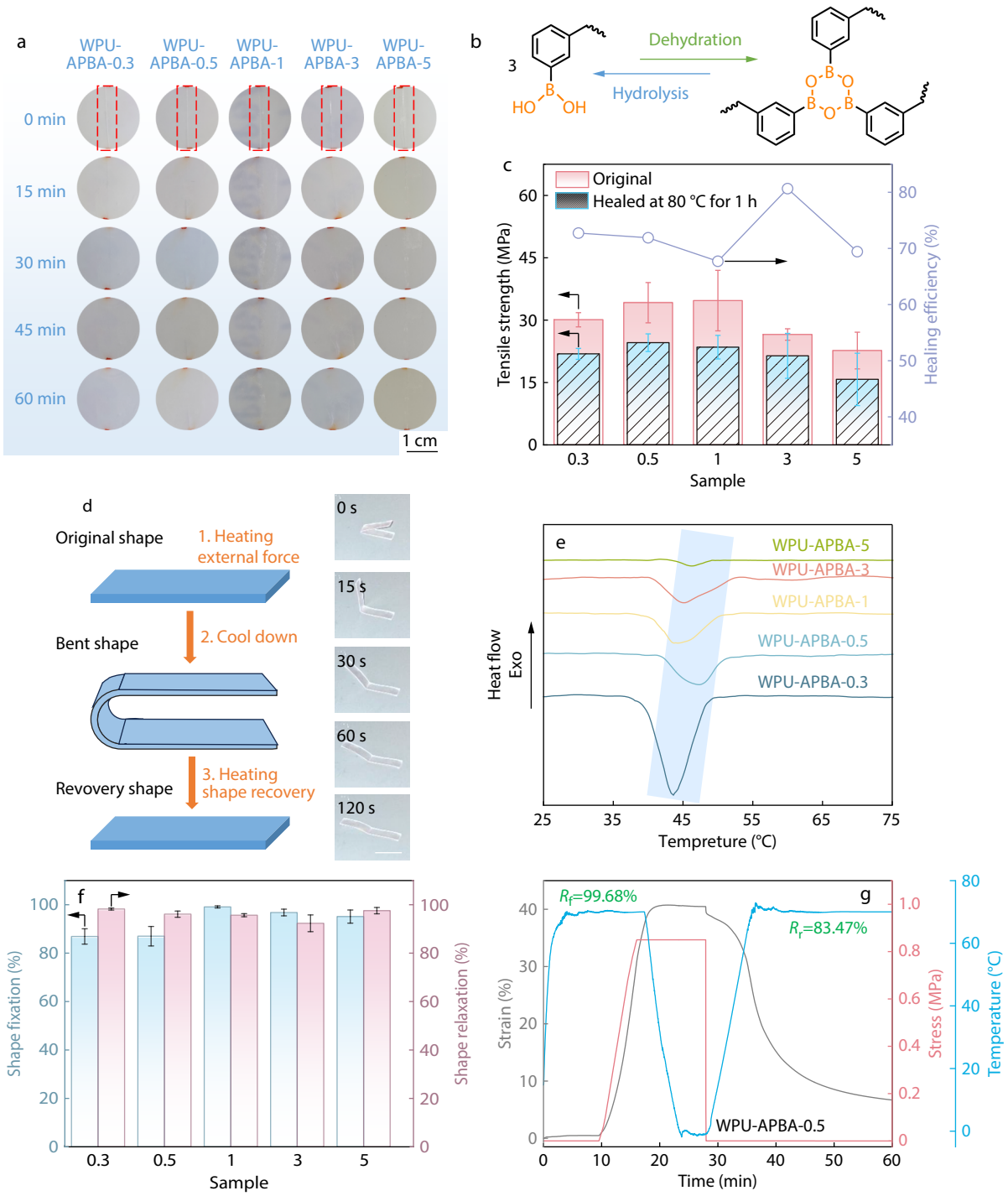


**Fig. 2** Self-healing and shape memory behavior of WPU-APBA films. (a) Photograph images showing surface scratch healing of WPU-APBA-*x* films at 80 °C over time; (b) Schematic diagram of boroxine-mediated reversible hydrolysis and re-crosslinking, enabling self-healing; (c) Tensile strength of WPU-APBA-*x* before and after healing and corresponding self-healing efficiency; (d) Programmable "U"-shape memory process and recovery sequence. The attached figure depicts the physical picture of the shape memory recovery process; (e) DSC thermograms of WPU-APBA-*x*; (f) Average values ± standard deviation of the shape fixation rate and shape relaxation of WPU-APBA-*x* over five consecutive cycles; (g) Representative stress-controlled shape memory cycle of WPU-APBA-0.5.

crosslinking restricts the chain diffusion required for effective healing.

The shape memory behavior arises from the dual-phase segmented structure. The IPDI/APBA hard domains function as permanent netpoints, whereas the semicrystalline PCL soft segments act as reversible switching domains. This structure of soft- and hard-segment phase separation results in WPU-APBA having good shape memory performance, and the specific shape memory process is shown in Fig. 2(d). Upon heating above $T_g$, the chain mobility increases, and temporary

shapes can be programmed under an external force. Cooling below $T_g$ fixes the temporary shape and reheating restores the permanent shape. Complete macroscopic recovery was achieved within 120 s. As shown in Fig. 2(e), the melting temperature ($T_m$) of the semi-crystalline PCL domains in the WPU-APBA chain was between 43 and 47 °C, which acts as a reversible physical cross-linking point for temporary shape fixation. Selecting 70 °C as the programming temperature, which is approximately 20 °C higher than the $T_m$ of PCL, ensures that the PCL crystals are completely melted. Simultaneously, the hard segment phase enters a highly elastic state, and the dynamic boron-oxygen heterocyclic network participates in shape fixation and recovery. To quantify the shape memory efficiency, two metrics, the shape fixation rate ($R_f$) and shape recovery rate ($R_r$), were used, as defined in Eqs. (1) and (2):[49,74–76]

$$R_f = \left[\frac{180° - \theta_f}{180°}\right] \times 100\% \quad (1)$$

$$R_r = \left[\frac{180° - \theta_r}{180°}\right] \times 100\% \quad (2)$$

where $\theta_f$ is the angle between the two straight ends of the curved sample measured after cooling (fixed shape) and $\theta_r$ is the angle measured after heating (recovery shape).

Fig. 2(f) and Fig. S13 (in ESI) present the results for the WPU-APBA-*x* over 5 consecutive cycles. The histograms represent the average values of 5 cycles, and the error bars represent the corresponding standard deviations. Specific data are presented in Table S5 (in ESI). The DMA cycle test showed that WPU-APBA-1 exhibited maximum $R_f$>98%, while $R_r$ for all samples ranged from 61.18% to 83.47% (Figs. 2f and 2g, Figs. S9–S12 in ESI). These results show that the synthesized WPU-APBA has good self-healing and stable shape-memory performance. Among all compositions, WPU-APBA-0.5 demonstrated the most balanced performance, combining 71.9% self-healing efficiency, 83.47% shape memory recovery rate, and 34.92 MPa tensile strength. Therefore, WPU-APBA-0.5 was selected for subsequent studies because it provides optimal mechanical robustness, reversible deformation capability, and self-healing functionality.

## Light-responsive Color Switching Behavior

To introduce time-dependent optical functionality into the optimized WPU-APBA-0.5 matrix, 2,2′-dinaphthylamine (CDP) was physically incorporated to impart photochromic properties, yielding composites denoted as APBA-CDP. CDP was selected because of its conjugated naphthalene framework and nitrogen-centered electron-donating structure, which enables light-induced intramolecular electron transfer and the formation of a colored radical or charge-transfer state under ultraviolet irradiation.[8,77,78] The tensile properties of the APBA-CDP films are shown in Fig. S14 (in ESI), indicating a slight reduction in the mechanical properties after dye incorporation. This is attributed to the tendency of the organic dye molecules to aggregate, forming stress concentration points within the material. Under material loading, cracks preferentially initiate and propagate at these sites, resulting in early fractures and reduced mechanical strength. Nevertheless, the tensile strength remained above 22 MPa, which is sufficient to support subsequent applications. The proposed photochromic mechanism is illustrated in Fig. 3(a). Upon 365 nm UV exposure, CDP undergoes an electronic transition from the ground state to an excited state, followed by non-radiative relaxation into a colored species, resulting in a visible color change in the polymer film. To evaluate the tunability of the photochromic response, different CDP loadings (0.1 wt%, 0.5 wt%, and 1.0 wt%) were incorporated into the WPU-APBA-0.5 matrix. As shown in Fig. 3(b), increasing the CDP concentration accelerated the color development rate and enhanced the color intensity under identical UV irradiation times. At 1.0 wt%, a distinct brown coloration appeared within 30–60 s, whereas lower concentrations exhibited slower color evolution. This concentration-dependent behavior confirms that the optical response can be precisely modulated by the dye content, providing a controllable parameter for a time-gated encryption design. To quantitatively analyze the color transition, the color difference ($\Delta E$) was calculated as a function of irradiation time (Fig. 3c). $\Delta E$ increased monotonically with UV exposure time for all concentrations, with higher CDP loadings exhibiting larger $\Delta E$ values at equivalent irradiation times. These results verify that the photochromic response is both time- and composition-dependent, enabling programmable optical output. The chromaticity evolution was further analyzed using a CIE 1931 color space diagram (Fig. 3d). The chromaticity coordinates shifted from the initial near-neutral region toward the red–brown region upon UV irradiation, visually confirming the systematic color transformation. The progressive and controllable migration in the color space demonstrates the feasibility of using irradiation time as an additional encryption parameter. Importantly, the incorporation of CDP did not compromise the mechanical integrity or shape memory performance of the APBA network. As shown in Fig. S15 (in ESI), the shape memory cycling stability remained above 94% recovery after 5 cycles, indicating that the photochromic functionality operates independently without disrupting the dynamic covalent network. The self-healing performance of APBA-CDP was evaluated, as shown in Fig. S16 and Table S6 (in ESI). The incorporation of dye did not significantly affect the self-healing efficiency of WPU-APBA, which remained between 79.8% and 83.56%.

## Multistep Shape-color Coupled 4D Encryption System

The integration of thermally triggered shape memory and UV-responsive photochromic properties enables the APBA-CDP films to function as programmable physical encryption platforms. The encryption strategy was based on two orthogonal stimuli: temperature (shape transformation) and UV irradiation (time-dependent color evolution). As illustrated in Fig. 4(a), encrypted patterns were first written onto the APBA-CDP films using a photomask method. The polyurethane emulsion was cast into a square 2 cm × 2 cm polytetrafluoroethylene (PTFE) mold to obtain uniform films. A patterned black mask was placed on the film surface and irradiated with 365 nm UV light, generating localized brown regions corresponding to the exposed areas. The resulting patterns were stable under ambient conditions, indicating that UV-induced color formation was effectively irreversible under normal operating conditions, which prevented unintended information erasure. A highly secure 3D encryption system was designed using the photochromic and shape memory properties, as shown in Fig. 4(b). The flat film was heated to 70 °C, mechanically rolled into a spiral geometry, and fixed at −20 °C. In this temporary configuration, encoded information is geometrically concealed and cannot be interpreted directly.

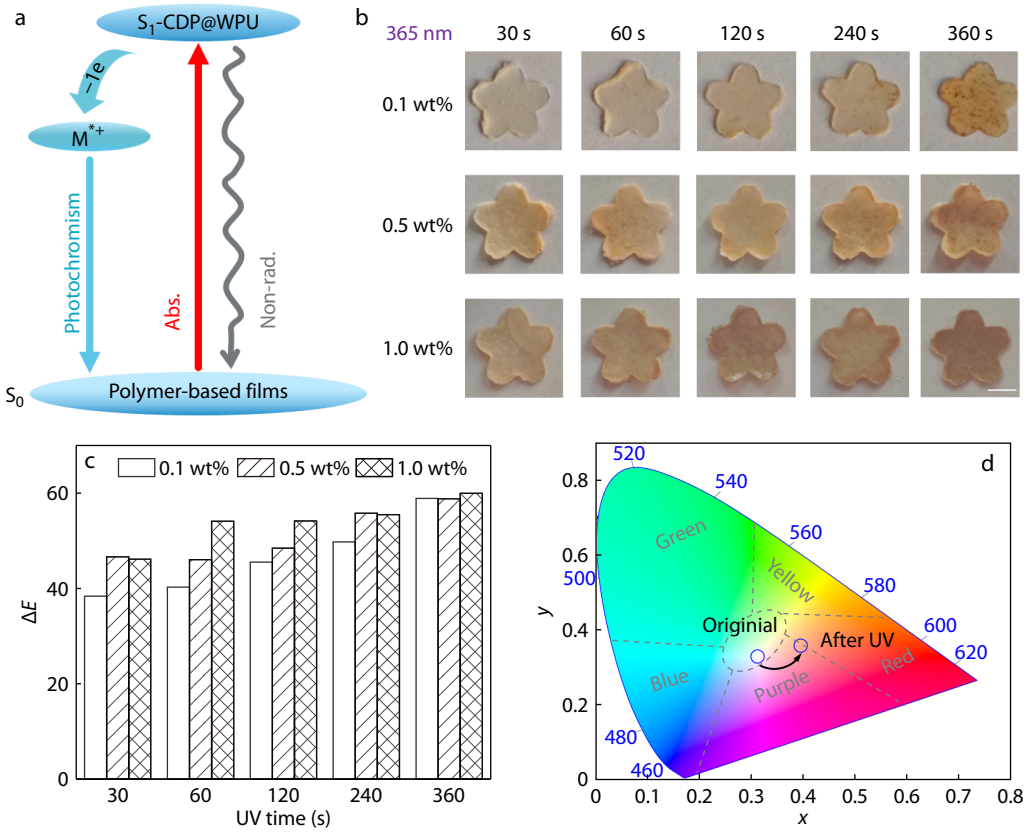


**Fig. 3** Photochromic behavior of APBA-CDP films. (a) Proposed UV-induced photochromic mechanism of CDP within the polyurethane matrix; (b) Time-dependent color evolution of films containing different CDP concentrations under 365 nm irradiation; (c) Quantitative color difference ($\Delta E$) as a function of UV irradiation time; (d) CIE 1931 chromaticity diagram of APBA-CDP films before and after UV exposure, showing systematic color shift.

During decryption, reheating to 70 °C restores the film to its original planar configuration, revealing the positioning markers that guide correct message reading. Using a Morse-based spatial encoding strategy, the message "HOPE" was successfully decoded. Subsequently, the extended UV irradiation permanently alters the optical state, serving as a controlled destruction step to prevent secondary information leakage. While this 3D encryption strategy increases security by coupling spatial geometry with optical encoding, static 3D systems remain theoretically vulnerable to replication once both the structure and the optical state are known. Therefore, an additional layer of encryption is required to further enhance resistance to reverse engineering.

To solve this possible risk of leakage, a fourth dimension, time, was introduced using irradiation duration as the core key to designing an advanced 4D encryption system. Because the CDP concentration governs the rate of color development, films with different CDP loadings exhibit distinct color evolution kinetics under identical UV exposure. By spatially integrating the APBA and APBA-CDP layers with varying dye concentrations, a time-resolved information output platform was constructed (Fig. 5). As shown in Fig. 5(a), the film was first preprogrammed into a spiral configuration *via* thermal deformation and fixation. After recovering to the planar state at 70 °C, the film was exposed to UV light. Because different regions contain different CDP concentrations (Fig. 5b), encoded patterns emerge sequentially, depending on the irradiation time. The decryption process is illustrated in Fig. 5(c). The spiral shape was heated at 70 °C to remove the 3D shape, and the color change was combined with the Moss code to enhance decryption difficulty and information density. The initial interference code in the first row reveals "A" and in the second row "T", forming "AT". After 30 s of continuous film irradiation at 365 nm, the second pattern emerges, with

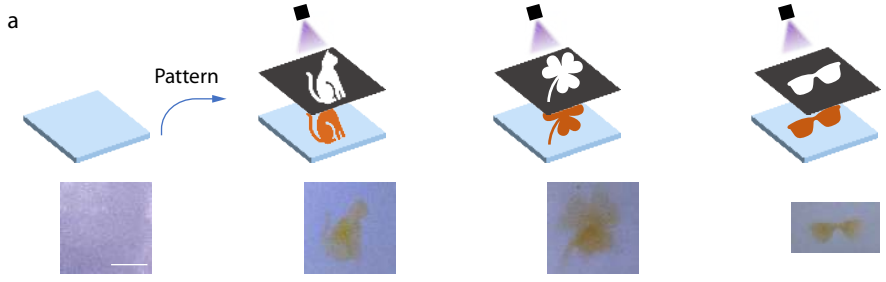


https://doi.org/10.1007/s10118-026-3722-6

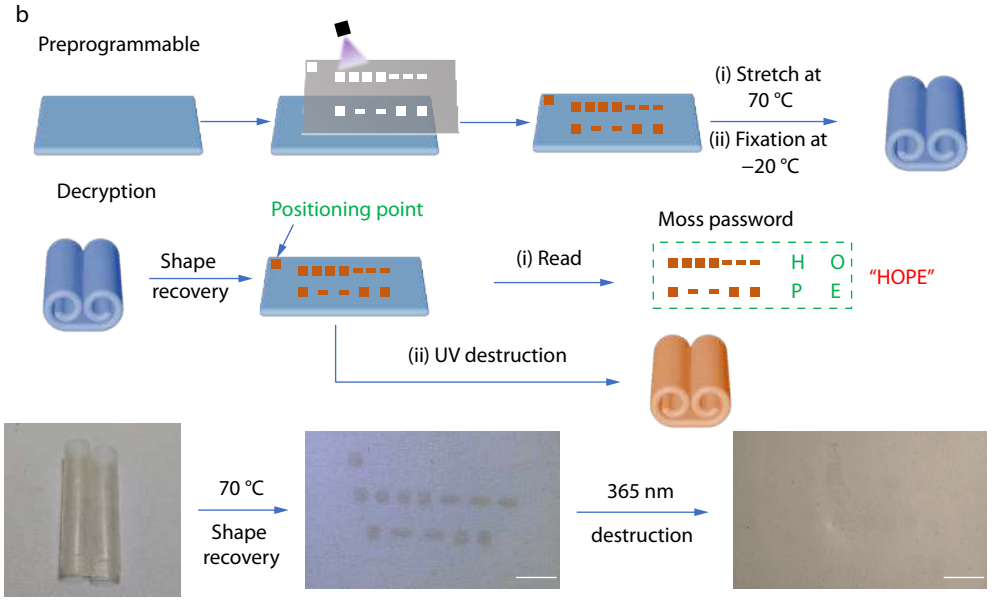


**Fig. 4** 3D encryption based on coupled shape memory and photochromism. (a) Pattern writing on APBA-CDP films using a photomask under 365 nm UV irradiation; (b) Encryption and decryption process: shape programming (70 °C deformation and −20 °C fixation), thermal recovery (70 °C), Morse-based decoding of the message "HOPE," and optional UV-triggered information destruction. (Scale bar=1 cm).

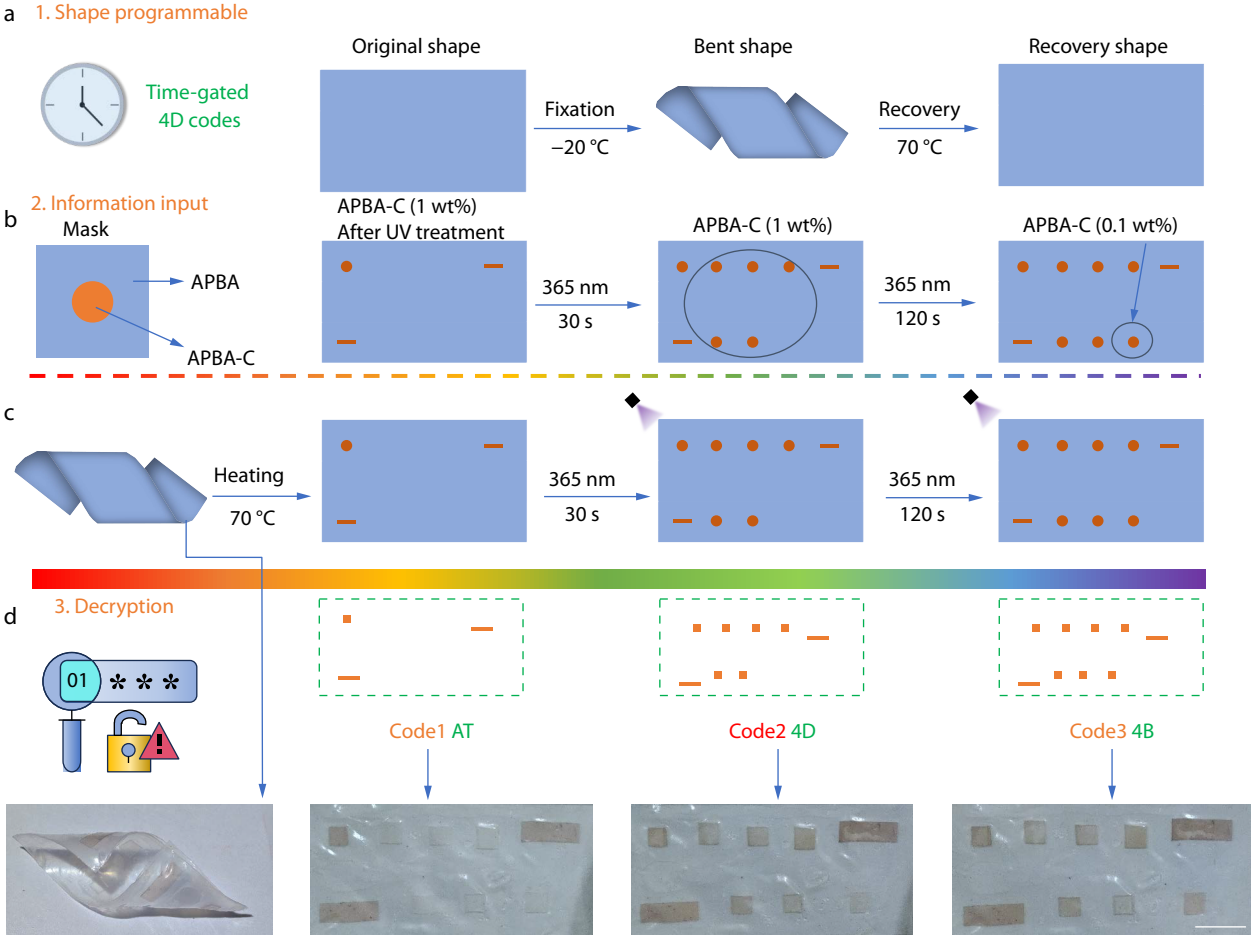


**Fig. 5** Time-gated 4D encryption strategy based on sequential shape recovery and UV-controlled color evolution. (a) Shape pre-programming of the film from flat to spiral configuration and recovery at 70 °C; (b) Spatial information input using APBA and APBA-CDP layers with different dye concentrations; (c) Time-gated 4D information encryption system with Morse cipher for secure message encoding; (d) Physical images of time-dependent message evolution. (Scale bar=1 cm).

https://doi.org/10.1007/s10118-026-3722-6

the first row reading "4" and the second row "D", forming the intermediate code "4D", which is the hidden correct information. Under continuous irradiation, a third decoy code appears at 120 s, with "4" on the first row and "B" on the second row, forming the final misleading code "4B". The decryption process for the physical image is illustrated in Fig. 5(d). Thus, only by applying the correct sequence, shape recovery followed by precisely timed UV irradiation could the intended information be extracted. Missing the correct irradiation window results in incomplete or misleading output. This time-gated strategy transforms the material from a static encryption carrier into a dynamically evolving system, significantly increasing decoding complexity. Unlike conventional systems that can be replicated once structural information is known, this platform requires accurate control of stimulus order, temperature, irradiation time, and spatial composition, thereby enhancing the resistance to brute-force simulation and reverse engineering.

## CONCLUSIONS

A dynamic covalent polyurethane network integrating shape memory, self-healing, and photochromic functionalities was prepared by incorporating APBA as a capping agent into WPU, followed by the physical incorporation of the photochromic dye CDP. The formation of reversible boroxine crosslinks provides stable network junctions that simultaneously serve as permanent netpoints for shape memory and dynamic sites for self-healing. The optimized WPU-APBA exhibited an excellent shape-fixity ratio of 99.68% and shape recovery ratio of 83.47%, together with a self-healing efficiency of up to 80.66% after heating at 80 °C for 60 min. The introduction of CDP endowed the material with controllable and time-dependent photochromic behavior under 365 nm irradiation, enabling programmable optical output without compromising mechanical integrity or shape memory performance. A sequential and time-gated 4D information encryption platform was realized by coupling thermally triggered shape recovery with UV-regulated color evolution. Information can be written, revealed, and intentionally destroyed through controlled stimulus sequences, significantly enhancing encryption complexity compared with conventional static systems. This study demonstrates a versatile material design strategy that integrates dynamic covalent chemistry with multimodal responsiveness, providing a promising approach for physical encryption, optical data storage, and advanced anti-counterfeiting applications.

### Conflict of Interests

The authors declare no interest conflict.

### Electronic Supplementary Information

Electronic supplementary information (ESI) is available free of charge in the online version of this article at http://doi.org/10.1007/s10118-026-3722-6.

### Data Availability Statement

The data supporting the findings of this study are available upon request from the corresponding author and are not publicly available because of privacy or ethical restrictions.

## ACKNOWLEDGMENTS

This work was financially supported by the National Natural Science Foundation of China (No. 22275023), Science Foundation of Jilin Province (No. 20260101017JJ), and Science and Technology Research Project of Jilin Provincial Department of Education (No. JJKH20240924KJ).

## REFERENCES

1 Wali, A.; Das, S. Hardware and information security primitives based on 2D materials and devices. *Adv. Mater.* **2023**, *35*, 2205365.
2 Aldhous, P. Murder by medicine. *Nature* **2005**, *434*, 132–134.
3 Butticè, V.; Caviggioli, F.; Franzoni, C.; Scellato, G.; Stryszowski, P.; Thumm, N. Counterfeiting in digital technologies: an empirical analysis of the economic performance and innovative activities of affected companies. *Res. Policy* **2020**, *49*, 103959.
4 Bhatt, P.; Valecha, R.; Rao, H. R. Situational awareness about data breaches and ransomware attacks: a multi-dimensional cyber threat impact framework and content analyses of practitioner-public discourses. *Int. J. Inf. Manage.* **2025**, *83*, 102902.
5 Miao, Y.; Chen, C.; Pan, L.; Han, Q. L.; Zhang, J.; Xiang, Y. Machine learning–based cyber attacks targeting on controlled information. *ACM Comput. Surv.* **2021**, *54*, 1–36.
6 Kudiabor, H. 'Anonymous' genetic databases vulnerable to privacy leaks. *Nature* **2024**, *634*, 764–765.
7 Shao, J.; Feng, S.; Liu, M.; Guo, Y.; Lu, C.; Ke, S.; Sun, H.; Tu, D.; Peng, D.; Zhang, Q.; Liu, F. Promising coloration composite strategy to multicolor photochromism for on-demand information displays. *Adv. Funct. Mater.* **2025**, *35*, 2425059.
8 Shan, M.; Li, A.; Wang, M.; Yang, Y.; Wang, J.; Yang, K.; Tang, B. Z.; Li, Z. Harnessing polymer matrices for tuning the luminescence and photochromism properties of organic photoresponsive materials. *ACS Mater. Lett.* **2025**, *7*, 1860–1868.
9 Li, B.; Zhang, Y.; Wang, J.; Yan, B.; Liang, J.; Dong, Y.; Zhou, Q. Fast and reversibly humidity-responsive fluorescence based on AIEgen proton transfer. *ACS Appl. Mater. Interfaces* **2022**, *14*, 49119–49127.
10 Yang, Y. F.; Bai, Y.; Li, Y. B.; He, C. F. Phase patterning of poly(oxime-ester) for information encryption by photo-induced isomerization. *Chinese J. Polym. Sci.* **2024**, *42*, 1488–1494.
11 Xu, L. R.; Wang, J. Y.; Huang, J. T.; He, Q. Y.; Lu, S. L.; Feng, D. C.; Ma, Z. T.; Yuan, Z. K.; Yang, Y. Z.; Chen, X. D. Multi-mode polarized luminescent au-nanorod polymer composites for advanced optical anti-counterfeiting. *Chinese J. Polym. Sci.* **2025**, *43*, 2118–2127.
12 Li, C.; Liu, J.; Qiu, X.; Yang, X.; Huang, X.; Zhang, X. Photoswitchable and reversible fluorescent eutectogels for conformal information encryption. *Angew. Chem. Int. Ed.* **2023**, *62*, e202313971.
13 Li, Y.; Li, H.; Jin, W.; Xu, X.; Liu, H.; Ding, Y.; Wang, G.; Zhang, T.; Peng, Q.; He, J.; Hu, Q.; Pan, L.; Li, K. $\pi$-$\pi$ Stacking controlled photochromic/thermochromic properties of salicylaldehyde schiff base in solid state. *Dyes Pigm.* **2022**, *202*, 110295.
14 Stal, S.; Huitorel, B.; Coustham, T.; Stephant, N.; Massuyeau, F.; Gacoin, T.; Bouteiller, L.; Perruchas, S. Photoactive CuI-cross-linked polyurethane materials. *ACS Appl. Mater. Interfaces* **2022**,

## Graphical Abstract

### Three-in-One Coupled Shape Memory, Self-healing, and Photochromic System in Dynamic Covalent Polyurethane Network for Sequential 4D Encryption

Yi-Xin Ji, Ahmed Olalekan Omoniyi, Yang Zhou, Ying-Chao Zhang, and Jian-Fu Zhang

*Changchun University of Science and Technology; Zhongshan Institute of Changchun University of Science and Technology; Weifang University of Science and Technology*

The three-in-one dynamic covalent polyurethane seamlessly couples shape memory, self-healing and photochromism to achieve high performance.

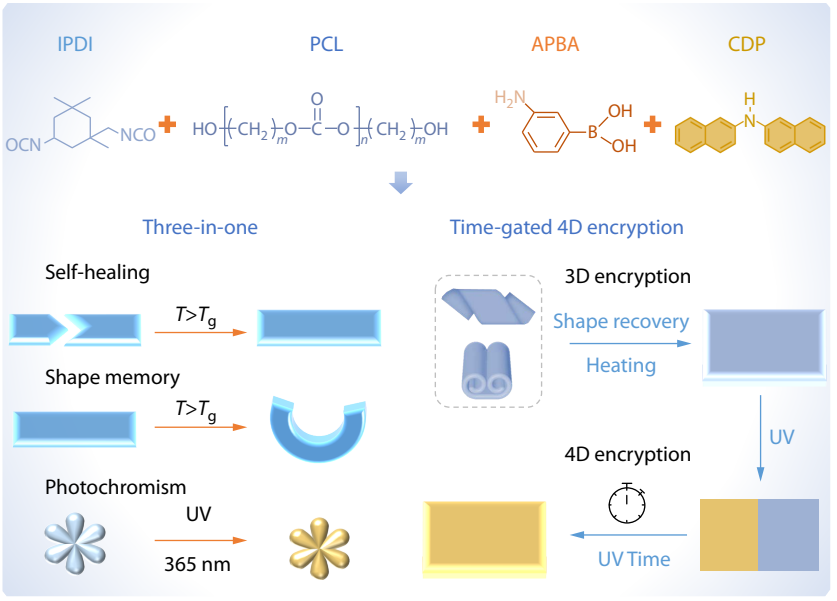


*Chinese J. Polym. Sci., 2026* *https://doi.org/10.1007/s10118-026-3722-6*

*14*, 47931–47940.

15 Guo, Z.; Bian, Y.; Zhang, L.; Zhang, J.; Sun, C.; Cui, D.; Lv, W.; Zheng, C.; Huang, W.; Chen, R. Multi-stimuli-responsive carbon dots with intrinsic photochromism and *in situ* radical afterglow. *Adv, Mater* **2024**, *36*, 2409361.

16 Ma, J. H.; Han, Y.; Guo, W. C.; Lu, H. Y.; Chen, C. F. Color-tunable thermally activated delayed fluorescence polymeric materials constructed by host–guest complexation revealing rewritable advanced information encryption. *CCS Chem.* **2024**, *7*, 2623–2632.

17 He, J.; Zang, Y.; Li, H.; Guo, J.; Wang, C. Humidity-responsive photonic system for security printing and information encryption. *Chem. Eng. J.* **2024**, *497*, 154838.

18 Lan, R.; Sun, J.; Shen, C.; Huang, R.; Zhang, L.; Yang, H. Reversibly and irreversibly humidity-responsive motion of liquid crystalline network gated by $SO_2$ gas. *Adv. Funct. Mater.* **2019**, *29*, 1900013.

19 Wang, Z.; Yuan, B.; Yang, Y.; Li, Z.; Zhang, Y.; Bao, J.; Zhang, L.; Lan, R.; Yang, H. Self-healable, shape-programmable and humidity-responsive liquid crystalline elastomer actuators enabled by dynamic covalent boronic ester bonds and aggregation induced emission luminogens. *Adv. Funct. Mater.* **2025**, *35*, 2421516.

20 Zhang, Z.; Wei, X.; Zhang, L.; Li, B. Visualization and depth estimation of inner crack in high-pressure equipment based on organic mechanochromic luminescent materials. *Adv. Mater. Interfaces* **2023**, *10*, 2300330.

21 Huang, Y.; Huang, S.; Li, Q. Mechanochromic polymers based on mechanophores. *ChemPlusChem* **2023**, *88*, e202300213.

22 Wang, Z.; Ma, Z.; Wang, Y.; Xu, Z.; Luo, Y.; Wei, Y.; Jia, X. A novel mechanochromic and photochromic polymer film: when rhodamine joins polyurethane. *Adv. Mater.* **2015**, *27*, 6469–6474.

23 Yu, C. J.; Yu, B. H.; Zeng, S. S. High humidity-resistant and reversible mechanochromic wrinkling surface activated by dual mechanical modes. *Chinese J. Polym. Sci.* **2025**, *43*, 1105–1113.

24 Wang, H.; Deng, H.; Chen, J.; Tian, Y.; Huang, F.; Zhao, Y.; Zhou, Z.; Cui, J.; Chen, J.; Chen, X. Self-growth of programmable 2D- and 3D-coupling responsive coating for anti-counterfeiting. *Nat. Commun.* **2026**, *17*, 1009.

25 Ma, M.; Dong, S.; Yuan, W.; Ma, T.; Xu, M.; Jiang, X.; Li, J. A programmable 2D/3D anti-counterfeiting system *via* shape memory polymer with surface wrinkle and fluorescence. *Adv. Funct. Mater.* **2024**, *35*, 2414467.

26 Pal, V.; Gupta, D.; Liu, S.; Namli, I.; Rizvi, S. H. A.; Yilmaz, Y. O.; Haugh, L.; Gerhard, E. M.; Ozbolat, I. T. Interparticle crosslinked ion-responsive microgels for 3D and 4D (bio)printing

applications. *Small* **2025**, *21*, e02262.
27 Guo, R.; Qi, W.; Liu, H.; Li, D.; Chen, G.; Li, Q.; Zhou, Z. Dynamic borate ester bond-based 3D printing fluorescence polysiloxane with self-healing, antimicrobial, and shape memory. *Chem. Eng. J.* **2024**, *485*, 149850.
28 Sun, H.; Maji, S.; Chandrakasan, A. P.; Marelli, B. Integrating biopolymer design with physical unclonable functions for anticounterfeiting and product traceability in agriculture. *Sci. Adv.* **2023**, *9*, eadf1978.
29 Klausen, M.; Zhang, J.; Stevens, M. M. Designing physical unclonable functions from optically active materials. *Adv. Mater.* **2025**, *37*, 2502059.
30 Du, L.; Zhang, H.; Wang, C.; Zhang, K.; Zhang, H.; Yang, J.; Wu, C.; Fan, Z.; Pan, L. Physical unclonable anti-counterfeiting "watermarks" *via* swelling-induced buckling-delamination in polymer bilayers for portable and robust authentication. *Adv. Funct. Mater.* **2025**, *36*, e15860.
31 Li, J.; Xie, S.; Meng, J.; Liu, Y.; Zhan, Q.; Zhang, Y.; Shui, L.; Zhou, G.; Feringa, B. L.; Chen, J. Dynamic control of multiple optical patterns of cholesteric liquid crystal microdroplets by light-driven molecular motors. *CCS Chem.* **2024**, *6*, 427–438.
32 Gao, J.; Wu, W.; Zhou, L.; Gong, S.; Li, C.; Chen, X.; Li, Y.; Li, K. Facile blinking dyes with spontaneous *enol-keto* tautomerism for super-resolution imaging of subcellular targets. *CCS Chem.* **2024**, *6*, 2770–2782.
33 Wang, Q.; Xu, H. ren; Li, X. hao; Qu, D. H. Temporal dynamic room-temperature phosphorescent materials with multicolor tunability for time-dependent information encryption. *CCS Chem*. **2025**, 1–10.
34 Liu, J.; Ji, Y.; Liu, X.; Omoniyi, A. O.; Yang, M.; Liang, Q.; Chen, D.; Zhou, Y.; Zhang, J.; Su, Z. 4D encryption system: hydrophilic–hydrophobic polyurethane actuators with smart color switching for high-capacity data storage. *Adv. Funct. Mater*. **2025**, *35*, 2501801.
35 Wu, Y.; Zhou, W.; Qiu, Y.; Wang, S.; Liu, J.; Chen, Y.; Xu, X.; Liu, Y. 4D assembly of time-dependent lanthanide supramolecular multicolor phosphorescence for encryption and visual sensing. *Adv. Sci*. **2025**, *12*, 2415418.
36 Ma, S.; Jiang, Z.; Wang, M.; Zhang, L.; Liang, Y.; Zhang, Z.; Ren, L.; Ren, L. 4D printing of PLA/PCL shape memory composites with controllable sequential deformation. *Bio-des. Manuf*. **2021**, *4*, 867–878.
37 Zuo, X.; Liu, C.; Hao, K.; Xu, M.; Liu, Y.; Wu, C.; Li, R.; Yu, R.; Huang, A.; Guo, J. 4D-printed fluorescent hydrogels for dual-encryption: Time-gated hierarchical morphing with multicolor fluorescence. *SmartMat* **2025**, *6*, e70043.
38 Wang, X.; Su, R.; Luo, S.; Han, S.; Yu, N.; Chen, X.; Gan, L.; Huang, J. Elastomeric intrinsic optical anti-counterfeiting with dual-color RTP from dual $n\rightarrow\pi^*$ transition and enhanced intersystem crossing. *Adv. Funct. Mater.* **2025**, *35*, e11543.
39 Du, L.; Dai, J.; Xu, Z. Y.; Yang, K. K.; Wang, Y. Z. From shape and color memory PCL network to access high security anti-counterfeit material. *Polymer* **2019**, *172*, 52–57.
40 Schmidt, C.; Neuking, K.; Eggeler, G. Functional fatigue of shape memory polymers. *Adv. Eng. Mater.* **2008**, *10*, 922–927.
41 Kong, Q.; Tan, Y.; Zhang, H.; Zhu, T.; Li, Y.; Xing, Y.; Wang, X. Mimosa-inspired body temperature-responsive shape memory polymer networks: High energy densities and multi-recyclability. *Adv. Sci.* **2024**, *11*, 2407596.
42 Qi, S.; Tian, X.; Yuan, W. High-stretchable solid–solid phase change aerogel surface-modified with Ni-MOF for efficient photothermal energy conversion-storage and thermal-induced shape programming. *Adv. Funct. Mater.* **2025**, *35*, 2508204.
43 Xiao, L. P.; Qiu, L. M.; Wu, Z.; Wang, G. J. Nature-inspired pH-responsive hydrogels with rapid and high contrast changes in color, fluorescence, and shape simultaneously. *Chinese J. Polym. Sci.* **2024**, *42*, 1758–1767.
44 Ji, B.; Qin, L.; Yu, Y. L. Dynamic structural colors in helical superstructures: From supramolecules to polymers. *Chinese J. Polym. Sci.* **2025**, *43*, 406–428.
45 Jiang, S.; Guo, D.; Lin, F.; Chen, J.; Miao, Y.; Huang, H.; Yang, J. W.; Qin, W.; Chi, Z. Time-dependent multicolor afterglow from dual persistent luminescence of fluorescence and phosphorescence in a UV-cured polyurethane matrix. *ACS Mater. Lett.* **2024**, *6*, 1371–1379.
46 Bie, Z.; Yang, W.; Chen, Y.; Zheng, C.; Ikeda, T.; Wang, J.; Jiang, L. Temperature-time-dependent dynamic pattern from multi-inks printing based on chiral helix superstructure. *Adv. Funct. Mater.* **2025**, *35*, 2424107.
47 Xie, Y.; Zhao, X.; Wang, H.; Tian, Y.; Liu, C.; Wu, J.; Cui, J.; Zhou, Z.; Chen, J.; Chen, X. Hydrogen bond-associated photo-fluorochromism for time-resolved information encryption and anti-counterfeiting. *Angew. Chem. Int. Ed.* **2025**, *64*, e202414846.
48 Frick, A.; Rochman, A. Characterization of TPU-elastomers by thermal analysis (DSC). *Polym. Test.* **2004**, *23*, 413–417.
49 Ur Rehman, H.; Chen, Y.; Hedenqvist, M. S.; Li, H.; Xue, W.; Guo, Y.; Guo, Y.; Duan, H.; Liu, H. Self-healing shape memory PUPCL copolymer with high cycle life. *Adv. Funct. Mater.* **2018**, *28*, 1704109.
50 Wu, G.; Panahi Sarmad, M.; Van Vlierberghe, S.; Xu, R.; Hou, X.; Cui, Z.; Xiao, X. Multi-stimuli responsive shape memory behavior of dual-switch TPU/CB/CNC hybrid nanocomposites as triggered by heat, water, ethanol, and pH. *Chem. Eng. J.* **2022**, *450*, 138253.
51 Wang, X.; Zhan, S.; Lu, Z.; Li, J.; Yang, X.; Qiao, Y.; Men, Y.; Sun, J. Healable, recyclable, and mechanically tough polyurethane elastomers with exceptional damage tolerance. *Adv. Mater.* **2020**, *32*, 2005759.
52 Yao, X.; Zhang, S.; Wei, N.; Qian, L.; Ding, H.; Liu, J.; Song, W.; Coseri, S. Poly(ionic liquid) functionalization: a general strategy for strong, tough, ionic conductive, and multifunctional polysaccharide hydrogels toward sensors. *SusMat* **2024**, *4*, e249.
53 Wang, Y.; Shu, R.; Zhang, X. Strong, supertough and self-healing biomimetic layered nanocomposites enabled by reversible interfacial polymer chain sliding. *Angew. Chem. Int. Ed.* **2023**, *62*, e202303446.
54 Yan, Z.H.; Huang, H.X.; Ding, G.Q.; Dong, S.S.; Jiang, K.J.; Li, Y.Y.; Liu, Y.; Jiang, Y.; Wang, S.F.; Hu, G.H.; Du, J.; Zhang, S.X.; Zhao, H. Research progress of high-strength self-healing polymer materials: Balance between mechanical strength and self-healing efficiency. *Chem. Eng. J.* **2025**, *518*, 164609.
55 Liu, M.; Zhong, J.; Li, Z.; Rong, J.; Yang, K.; Zhou, J.; Shen, L.; Gao, F.; Huang, X.; He, H. A high stiffness and self-healable polyurethane based on disulfide bonds and hydrogen bonding. *Eur. Polym. J.* **2020**, *124*, 109475.
56 Sokjorhor, J.; Phantan, C.; Ratanathawornkit, K.; Crespy, D. Simultaneous self-healing and corrosion protection using disulfide bonds. *Adv. Funct. Mater.* **2025**, *35*, 2508274.
57 Liang, S.; Wang, P.; Sun, Z.; An, H.; Wang, X.; Li, N. Microcrack self-healing capability of waterborne polyurethane/polyacrylate composites with dynamic disulfide bond. *J. Appl. Polym. Sci.* **2023**, *140*, e53744.
58 Fang, X.; Tian, N.; Hu, W.; Qing, Y.; Wang, H.; Gao, X.; Qin, Y.; Sun, J. Dynamically cross-linking soybean oil and low-molecular-weight polylactic acid toward mechanically robust, degradable, and recyclable supramolecular plastics. *Adv. Funct. Mater.* **2022**, *32*, 2208623.
59 Bao, C.; Guo, Z.; Sun, H.; Sun, J. Nitrogen-coordinated boroxines enable the fabrication of mechanically robust supramolecular thermosets capable of healing and recycling under mild conditions. *ACS Appl. Mater. Interfaces* **2019**, *11*, 9478–9486.

60 Gao, X.; Fang, X.; Wang, H.; Tian, N.; Sun, J. Fully erasable amphibious adhesives derived from soybean oil with record-high underwater adhesion strength. *Adv. Mater.* **2025**, *37*, e07894.
61 Yang, Y.; Davydovich, D.; Hornat, C. C.; Liu, X.; Urban, M. W. Leaf-inspired self-healing polymers. *Chem* **2018**, *4*, 1928–1936.
62 Zhang, Z.; Ghezawi, N.; Li, B.; Ge, S.; Zhao, S.; Saito, T.; Hun, D.; Cao, P.F. Autonomous self-healing elastomers with unprecedented adhesion force. *Adv. Funct. Mater.* **2021**, *31*, 2006298.
63 Zeng, F.; Ning, J.; Yang, Y.; Tian, C.; Huang, L.; Zhao, F.; Liu, Q.; Cui, M.; Lv, J.; Jiang, Y.; Cai, X.; Kong, W. A photohealable polyurethane with superior robustness and healing ratio. *Macromolecules* **2022**, *55*, 8741–8748.
64 Zhang, F.; Xiong, L.; Ai, Y.; Liang, Z.; Liang, Q. Str*et*chable multiresponsive hydrogel with actuatable, shape memory, and self-healing properties. *Adv. Sci.* **2018**, *5*, 1800450.
65 Liu, X.; Wu, J.; Tang, Z.; Wu, J.; Huang, Z.; Yin, X.; Du, J.; Lin, X.; Lin, W.; Yi, G. Photoreversible bond-based shape memory polyurethanes with light-induced self-healing, recyclability, and 3D fluorescence encryption. *ACS Appl. Mater. Interfaces* **2022**, *14*, 33829–33841.
66 Wang, X.; Xu, J.; Zhang, Y.; Wang, T.; Wang, Q.; Li, S.; Yang, Z.; Zhang, X. A str*et*chable, mechanically robust polymer exhibiting shape-memory-assisted self-healing and clustering-triggered emission. *Nat. Commun.* **2023**, *14*, 4712.
67 Peak, D.; Luther, G. W.; Sparks, D. L. ATR-FTIR spectroscopic studies of boric acid adsorption on hydrous ferric oxide. *Geochim. Cosmochim. Acta* **2003**, *67*, 2551–2560.
68 Brame, E. G.; Ferguson, R. C.; Thomas, G. J. Identification of polyurethanes by high resolution nuclear magnetic resonance spectrometry. *Anal. Chem.* **1967**, *39*, 517–521.
69 Li, Z.; Zhu, Y.; Niu, W.; Yang, X.; Jiang, Z.; Lu, Z.; Liu, X.; Sun, J. Healable and recyclable elastomers with record-high mechanical robustness, unprecedented crack tolerance, and superhigh elastic restorability. *Adv. Mater.* **2021**, *33*, 2101498.
70 Xue, Y.; Lin, J.; Wan, T.; Luo, Y.; Ma, Z.; Zhou, Y.; Tuten, B. T.; Zhang, M.; Tao, X.; Song, P. Str*et*chable, ultratough, and intrinsically self-extinguishing elastomers with desirable recyclability. *Adv. Sci.* **2023**, *10*, 2207268.
71 Guo, R.; Zhang, Q.; Wu, Y.; Chen, H.; Liu, Y.; Wang, J.; Duan, X.; Chen, Q.; Ge, Z.; Zhang, Y. Extremely strong and tough biodegradable poly(urethane) elastomers with unprecedented crack tolerance *via* hierarchical hydrogen-bonding interactions. *Adv. Mater.* **2023**, *35*, 2212130.
72 Yang, Y.; Du, F.; Li, Z.; Thermally healable and reprocessable polymethacrylate networks based on diol-mediated metathesis of 6-membered boronic esters. *Polym. Chem*. **2020**, *11*, 1861–1870.
73 Soman, B.; Kyung Go, Y.; Shen, C.; Leal, C.; M. Evans, C. Impact of dynamic covalent chemistry and precise linker length on crystallization kinetics and morphology in ethylene vitrimers. *Soft Matter* **2022**, *18*, 293–303.
74 Song, C.; Zhang, Y.; Bao, J.; Wang, Z.; Zhang, L.; Sun, J.; Lan, R.; Yu, Z.; Zhu, S.; Yang, H. Light-responsive programmable shape-memory soft actuator based on liquid crystalline polymer/polyurethane network. *Adv. Funct. Mater.* **2023**, *33*, 2213771.
75 Yue, X.; Dong, C.; Wang, Y.; Cui, Z.; Ren, Z.; Guan, Z. H. Three birds with one stone: design and synthesis of polyurethane actuator for executing heat, light and humidity triggered deformation. *Chem. Eng. J.* **2023**, *457*, 141290.
76 Ping, P.; Wang, W.; Chen, X.; Jing, X. Poly(epsilon-caprolactone) polyurethane and its shape-memory property. *Biomacromolecules* **2005**, *6*, 587–592.
77 Kopcsik, E.; Mucsi, Z.; Kontra, B.; Vanyorek, L.; Gál, R.; Viskolcz, B.; Nagy, M. Excited state iminium form can explain the unexpected solvatochromic behavior of symmetric 1,5- and 1,8-diaminonaphthalenes. *Chem. Commun.* **2024**, *60*, 1008–1011.
78 Wang, S.; Cai, J.; Sadygov, R.; Lim, E. C. Intramolecular charge transfer and solvent-polarity dependence of radiative decay rate in photoexcited dinaphthylamines. *J. Phys. Chem.* **1995**, *99*, 7416–7420.


https://doi.org/10.1007/s10118-026-3722-6